

Refinement and Structural Analysis of Bovine Cytochrome b_5 at 1.5 Å Resolution

ROSEMARY C. E. DURLEY AND F. SCOTT MATHEWS

Department of Biochemistry and Molecular Biology, Washington University School of Medicine,
660 S. Euclid Avenue, Box 8231, St. Louis, MO 63110, USA

(Received 13 February 1995; accepted 13 June 1995)

Abstract

The structure of bovine liver cytochrome b_5 , a soluble 93-residue proteolytic fragment of a 16 kDa. membrane-bound hemoprotein, initially solved at 2.0 Å resolution, has been refined at 1.5 Å using data collected on a diffractometer. Refinement to 2.0 Å resolution used the Hendrickson–Konert procedure *PROLSQ* and was then extended to 1.5 Å resolution using the program *PROFFT*. Only residues 3–87 could be identified in the model and these residues together with 93 water molecules gave an agreement factor of $R = 0.161$ for data in the resolution range 1.5–5 Å. The structure was finally refined using the program *X-PLOR*, which enabled alternate conformers to be modelled for several surface side chains. Residues 1 and 2 at the amino terminus of the protein and residue 88 near the carboxyl terminus could be identified from these electron-density maps. However the remaining disordered carboxy-terminal residues could not successfully be included in the model. A total of 117 solvent molecules were included in the final refinement to give $R = 0.164$ for the data between 1.5 and 10 Å.

1. Introduction

Cytochrome b_5 is an electron-transfer protein found in a variety of cell types and intracellular locations (Strittmatter & Velick, 1956; Mathews & Czerwinski, 1985). It serves at least three known functional roles. The most thoroughly studied function is in membrane biosynthesis where it provides reducing equivalents to a fatty acid desaturase located in the endoplasmic reticulum of liver cells (Oshino, Imai & Sato, 1971; Holloway & Katz, 1972). A second function is to act as a reductant for mammalian cytochrome P_{450} , also in liver cells (Estabrook, Hildebrandt, Baron, Netter & Leibman, 1971; Enoch & Strittmatter, 1979). In both these functional roles cytochrome b_5 is an integral membrane protein and accepts electrons from a specific NADH-linked cytochrome b_5 reductase (Rogers & Strittmatter, 1975), also membrane bound. The third well characterized function of cytochrome b_5 is as a methemoglobin reductase in erythrocytes (Hultquist & Passon, 1971; Slaughter, Williams & Hultquist, 1982; Hegesh, Hegesh & Kaftory, 1986). In this role the cytochrome b_5 is in soluble form, as is the corresponding NADH-cytochrome b_5 reductase.

A similar soluble cytochrome b_5 – b_5 reductase system has also been identified in sipuncular erythrocytes where it serves to reduce methemerythrin (Utecht & Kurtz, 1988).

The membrane-bound form of cytochrome b_5 has molecular weight of about 16 kDa. and consists of about 130 amino-acid residues (Spatz & Strittmatter, 1971). It contains heme IX bound non-covalently. The protein is believed to comprise two domains, a hydrophilic domain consisting of approximately the first 100 amino acids and a hydrophobic domain containing the remaining 30 residues (Dailey & Strittmatter, 1979). The hydrophilic domain contains the heme group while the hydrophobic domain serves to anchor the protein to the membrane surface. The hydrophilic domain of cytochrome b_5 can be released from membranes by the action of a number of proteolytic enzymes. Treatment of liver microsomes by trypsin results in the solubilization of an 84-residue cytochrome b_5 which is resistant to further proteolysis (Strittmatter & Ozols, 1966).

The complete amino-acid sequence of cytochrome b_5 , from a number of mammalian species, has been determined (Ozols, Gerard & Nobrega, 1976). The DNA sequences from bovine, rabbit and human cDNA libraries have corrected several errors in the earlier amino-acid sequences (Miyata, Nagata, Yamazoe & Kato, 1989; Yoo & Steggles, 1988). In addition the cytochrome b_5 corresponding to the rat and the bovine amino-acid sequences, as well as several mutant forms, have been expressed in *Escherichia coli* using fully synthetic genomic material (Beck von Bodman, Schuler, Jollie & Sligar, 1986; Funk *et al.*, 1990).

The amino-acid sequences of the soluble portions of the mammalian cytochrome b_5 's are highly conserved having about 90% sequence identity and no insertions (Mathews, 1985). In addition, there are several other b -type cytochrome fragments which show distinct sequence similarity to mammalian cytochrome b_5 , including rat outer membrane mitochondrial b_5 (Lederer, Shrir, Guiard, Cortial & Ito, 1983) and the cytochrome domains from flavocytochrome b_2 (Guiard, Groudinsky & Lederer, 1974), sulfite oxidase (Guiard & Lederer, 1979a) and assimilatory nitrite reductase (Le & Lederer, 1983). These sequences are approximately 30% identical to one another, indicating an evolutionary relationship between them and suggesting the occurrence of a com-

mon structural motif, the 'cytochrome b_5 fold' (Guiard & Lederer, 1979b).

The crystal structure of bovine cytochrome b_5 was first determined at 2.8 Å resolution (Mathews, Levine & Argos, 1972) by multiple isomorphous replacement (MIR) and was extended to 2.0 Å resolution (Mathews, Argos & Levine, 1971). In the electron-density map only the segment from positions 3 to 87 could be located, even though the isolated protein prior to crystallization contained 93 amino acids. The remainder of the protein was thought to be disordered or possibly cleaved by further proteolysis prior to or during crystallization. The structure of a recombinant, triple mutant of bovine cytochrome b_5 has also been reported (Funk *et al.*, 1990). The present paper describes the refinement of the native bovine cytochrome b_5 at 1.5 Å resolution.

2. Experimental

2.1. Data collection

The crystals of cytochrome b_5 belong to space group $P2_12_12_1$ with unit-cell parameters $a = 64.54$, $b = 46.04$ and $c = 29.91$ Å and were kindly provided by Dr Philip Strittmatter. Data had been collected to 2.0 Å resolution from four crystals on a Picker diffractometer and merged as described previously (Mathews *et al.*, 1971).

Additional data were recorded for the resolution range 2.2–1.5 Å, from a new single crystal, on the Picker diffractometer. One observation was made of each reflection. The data were corrected for L_p , radiation damage and absorption as described previously (Mathews *et al.*, 1972). A total of 13 356 possible reflections were recorded in this resolution range. Only those reflections with intensities greater than twice the standard deviation were retained. The data were scaled to the previous 2.0 Å resolution data and merged with them. The total number of reflections obtained in this way was 9843. Table 1 gives the fractional distribution of observed reflections as a function of resolution.

2.2. Refinement

The atomic coordinates, obtained from a Richards Box (Richards, 1968), were refined in real space (Diamond, 1971) for two cycles using the 2.0 Å resolution electron-density map (Mathews, Czerwinski & Argos, 1979). 23 cycles of refinement were then carried out in the resolution range 5.0–2.0 Å using the Hendrickson–Konnert program *PROLSQ* (Hendrickson & Konnert, 1980) with constant weights applied to all the observations. No model rebuilding was carried out, nor were any water molecules introduced into the model. At this stage the R factor was 0.218 and the root-mean-square deviation from ideality (r.m.s.d.), for the model, was 0.025 Å.

Refinement was continued using the program *PROFFT* (Finzel, 1987), a version of *PROLSQ* which utilizes a fast fourier transform-based algorithm for

Table 1. Fractional distribution of observed reflections, in resolution ranges, with intensity greater than 2σ

Resolution (Å)	Percentage
50–2.0	99.2
2.0–1.9	72.9
1.9–1.8	60.3
1.8–1.7	45.1
1.7–1.6	29.1
1.6–1.5	16.5

structure-factor calculation. The model was periodically rebuilt on a graphics system and solvent molecules were gradually incorporated. The resolution of the refinement was gradually extended to the final value of 1.5 Å. A total of 105 cycles of *PROFFT* refinement was carried out in 16 stages. The various stages of refinement are summarized in Table 2(a). In each stage, several cycles of stereochemically restrained least squares refinement were carried out; after which electron-density maps were calculated, using both $F_o - F_c$ and $2F_o - F_c$ as coefficients, and examined on an IRIS interactive graphics system using Alberta/Caltech *TOM*, based on *FRODO* (Jones, 1985) or *TURBO* (Roussel & Cambillau, 1991).

During the initial stages of refinement the conformation of the backbone was restrained to have five atoms of the peptide unit, $C_{i\alpha}$, C_i , O_i , N_{i+1} and $C_{i+1\alpha}$, lie in a single plane. The distances of the Fe atom to the pyrrole N atoms of the heme and the ND atoms of the two histidine ligands were also restrained. After stage 9 the restraints on the Fe atom to ligand distances were removed along with the peptide coplanarity restraint on backbone atoms $C_{i+1\alpha}$. In general the target restraints were those outlined by Hendrickson & Konnert (1980).

Solvent sites were included in the model with neutral O atoms representing water molecules. All solvent sites were attributed to water and assigned unit occupancy. Initially solvent sites were included only if the solvent formed direct hydrogen bonds to the protein. Later sites were included which had reasonable hydrogen bonds to other water molecules. No isolated peaks were modelled as solvent. The initial temperature factor assigned for each solvent site depended on its peak height in the difference map and ranged from 20 to 35 Å². During the refinement a solvent site was re-examined on the graphics system if the temperature factor went above 40 Å². If the hydrogen bonding seemed reasonable then the site was retained. Before the last six cycles of this refinement four water sites with temperature factors greater than 45 Å² were removed. Although the density for residues 3 and 87 was clear, there were no indications of continuation of the peptide chain either at the amino or carboxy terminus of the polypeptide.

The convergence of the cytochrome b_5 refinement using *PROFFT* was extremely sensitive to the weighting scheme. During the first stage of refinement unit weights

Table 2. Synopses of *PROFFT* and *X-PLOR* refinement of cytochrome *b₅*(a) *PROFFT* refinement

Stage	No. of cycles	Resolution (Å)	Final <i>R</i> factor	R.m.s.d. (Å)	Comments
		10–2.0	0.284		Starting model.
1	9	10–2.0	0.262	0.045	No solvent sites, overall <i>B</i> factor, constant weights.
2	5	10–1.8	0.264		Tightened restraints, linear weighting.
3	3	10–1.8	0.238	0.039	Individual <i>B</i> factors refined.
4	6	10–1.8	0.218	0.039	14 solvent sites added.
5	5	10–1.8	0.220	0.020	A new weighting scheme, tightened restraints.
6	11	5–1.6	0.210	0.023	22 solvent sites
7	6	5–1.6	0.200		45 solvent sites.
8	7	5–1.6	0.188	0.023	54 solvent sites. Omit maps were computed.
9	14	5–1.56	0.182	0.009	65 solvent sites.
10	9	5–1.56	0.178	0.009	62 solvent sites. Removed restraints on heme Fe, relaxed restraints on peptide planarity (see text).
11	4	8–1.56	0.176	0.009	69 solvent sites.
12	9	5–1.55	0.169	0.006	83 solvent sites.
13	7	5–1.50	0.166	0.005	86 solvent sites.
14	4	5–1.50	0.164	0.005	87 solvent sites. Histidine 15 was 'flipped'.
15	6	5–1.50	0.161	0.005	91 solvent sites.

(b) *X-PLOR* refinement

Stage	No. of scatterers	Resolution (Å)	Final <i>R</i> factor	Comments
	736	5–1.5		Starting model, no solvent, <i>R</i> = 0.17.
	736	8–1.5		Resolution used for initial refinement, <i>R</i> = 0.22.
1	736	8–1.5	0.220	Simulated annealing, temp 3000–200 K followed by 100 cycles of positional refinement. Electron-density maps calculated.
2	770	8–1.5	0.184	Initial <i>R</i> = 0.20. 34 solvent sites added. Positional refinement followed by restrained refinement of individual <i>B</i> factors.
3	796	8–1.5	0.173	60 water sites included.
4	837	8–1.5	0.169	Alternate positions added for the side-chains of Lys19 and Glu69. 91 Solvent sites included in the model. Reduced all energy constraints on the heme iron.
5	860	12–1.5	0.176	Ran a series of SA omit maps for the 44, 66–69, 19 and 56 regions of the structure. Residues 1–90 with Glu56 modelled as Ala. 92 waters and alternate positions for side chains 19, 44, 48 and 69. Sorted waters by <i>B</i> factors. R.m.s.d. 0.009 Å and 1.99°.
6	908	12–1.5	0.167	Poor refinement of Pro90, each map gives different density. Only 1–89 included and 89 modelled as Ala. 108 waters and alternate positions for 2, 48, 61, 66, 69 and 75.
7	892	10–1.5	0.164	Conservative model, residues 1–88, 117 waters sites, alternate positions only for side chains of Glu48, Val61, Glu69 and Ile75. Partial occupancy for residues 1 and 2.

for the structure factors were used, for all reflections. Later a resolution-dependent weighting scheme was used where $w_F = 1/\langle\sigma_F\rangle_c^2$ and $\langle\sigma_F\rangle_c$ is an approximation to σ_F , the standard deviation of the structure factor. The quantity $\langle\sigma_F\rangle_c$ is a linear function of resolution equal to $A\sigma_F + B\sigma_F(\sin\theta/\lambda - 1/6)$. The terms $A\sigma_F$ and $B\sigma_F$ are obtained from a least-squares fit of $\langle\sigma_F\rangle_c$ to $|F_o - F_c|$ at each refinement cycle but can be altered at any stage of refinement. The values of $A\sigma_F$ and $B\sigma_F$ used for the last eight cycles of refinement were approximately 90 and 77% of the suggested values. The synopsis of this refinement is given in Table 2(a).*

At the end of the *PROFFT* refinement several surface side chains of the protein appeared to have multiple

conformations. Therefore, it was decided to continue refinement using the *X-PLOR* molecular dynamics refinement package (Brünger, 1990) and attempt to model the disordered groups. Simulated annealing (SA) was performed to reduce bias in the model (Hodel, Kim & Brünger, 1992); no solvent sites were included from the *PROFFT* refinement. The initial *R* factor was 0.17 for the resolution range 5–1.5 Å and 0.22 for the range 8–1.5 Å. The model, consisting of 736 scatterers, was subjected to one cycle of SA followed by positional refinement.

Solvent molecule positions were redetermined from the $F_o - F_c$ and $2F_o - F_c$ maps. The procedure of positional refinement, map calculation, model rebuilding and addition of solvent was continued until 60 waters had been included and the *R* factor had dropped to 0.18. At this stage a second conformer was added for two residues together with an additional 31 waters. Several additional side chains with multiple conformations were then identified. The models included alternate positions only for side chains with two distinct conformations.

* Atomic coordinates and structure factors have been deposited with the Protein Data Bank, Brookhaven National Laboratory (Reference: 3B5C for the *PROFFT* refinement, 1CYO for the *X-PLOR* refinement). Free copies may be obtained through The Managing Editor, International Union of Crystallography, 5 Abbey Square, Chester CH1 2HU, England (Reference: SX0001).

For more poorly ordered side chains only the principal conformer was retained and the occupancy was reduced.

After 91 waters had been included in the refinement and the R factor was below 0.17, it was noted that considerable density surrounded the first and last residues of the model. The density close to Ala3 could be modelled as two residues, Ser1 and Lys2. The density for the side chain of the lysine was weak and branched at $C\alpha$, $C\beta$ and $C\gamma$. However one orientation was stronger than all the others and this was used for further refinement. The density at the carboxy terminus was much more difficult to interpret as the remaining six residues. Many attempts were made to fit this density and some of the models were refined. However in the final model only Thr88 has been included. A summary of the X -PLOR refinement is given in Table 2(b).

The final model of cytochrome b_5 contains 892 scatterers, including 117 waters, and has an R factor of 0.164 for data in the 10–1.5 Å range. The r.m.s.d. for bond lengths is 0.009 Å and for bond angles is 1.2°. The model includes alternate positions for the side chains of residues Glu48, Val61, Glu69 and Ile75. The relative occupancies of these positions were not refined but were assigned on the basis of their electron density.

3. Results and discussion

3.1. Least-squares refinement

The amino-acid sequence of cytochrome b_5 is shown in Fig. 1. Included in the figure are the locations of six

Table 3. Statistics of the final model as refined by X -PLOR

Resolution range (Å)	1.5–10
Reflections used for refinement	9541
Number of atoms	
Total non-H atoms	892
Principal conformation only	874
Solvent O atoms	117
Average B factors (Å ²)	
For protein	15
For heme	12
For solvent waters	39
R.m.s.d.	
Bonds (Å)	0.009
Angles (°)	1.2
Standard R factor*	0.164

* Standard R factor = $\sum |F_o| - |F_c| / |F_o|$.

helices, five β -strands and the two ligands to the heme. Also indicated is the C-terminal segment of the protein sequence which could not be modelled in the electron density. A statistical summary of the final model is presented in Table 3. A plot of R factor versus resolution (Luzzati, 1952) is shown in Fig. 2, a Ramachandran plot (Ramakrishnan & Ramachandran, 1965) in Fig. 3 and the distribution of average main-chain and side-chain temperature factors, for the principal conformers, is shown in Fig. 4.

The initial refinement at 2.0 Å resolution using $PROLSQ$ gave a good starting model for further refine-

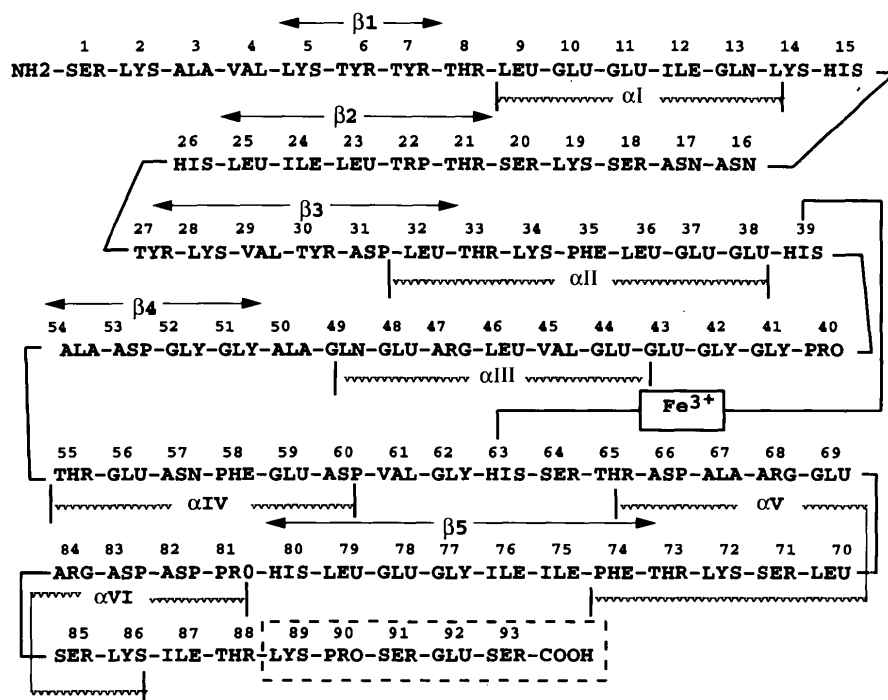


Fig. 1. The amino-acid sequence of calf liver cytochrome b_5 . Secondary structure is indicated schematically along with the heme coordination. The dashed box indicates the residues which could not be modelled into the electron density.

ment at higher resolution. Continued refinement using the program *PROFFT* led to gradual improvement of the structure with the eventual extension to 1.5 Å resolution. The advantage of using *PROFFT* over *PROLSQ* was the greatly increased speed of computation. The model of cytochrome *b*₅ obtained from this refinement was highly restrained, having r.m.s.d. of 0.005 Å and an *R* factor of 0.161 for the 5.0–1.5 Å resolution range. Throughout the

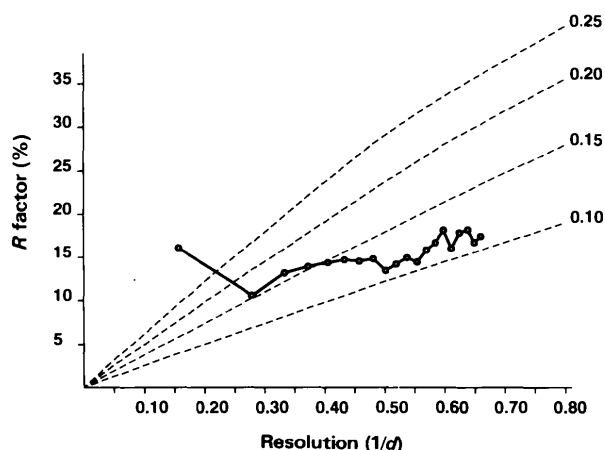


Fig. 2. Luzzati plot of *R* versus resolution for the 1.5 Å refined model of cytochrome *b*₅.

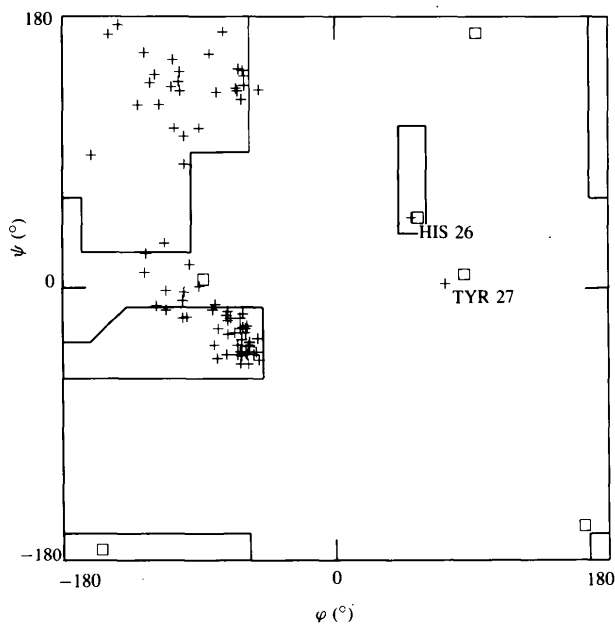


Fig. 3. Ramachandran plot of the 1.5 Å model of cytochrome *b*₅. Glycine residues are represented by squares. 91% of the residues have conformations in the most favored regions and the remaining 9% are in the generously allowed regions (Morris, MacArthur, Hutchinson & Thornton, 1992).

refinement difference maps were calculated, examined and the model rebuilt when required. Model rebuilding was primarily localized to the problem areas of the structure, notably, the N and C termini and the side chains of several short polypeptide segments, 17–19, 26–28, 43–44, 47–48 and residue 69. All of these side chains, which lie on or near the surface, had relatively large thermal parameters (Fig. 4). There was some evidence from omit maps of dual conformers for the side chains of residues Glu69 and Lys28. No alternate conformation was refined using *PROFFT*.

During the course of analysis, it was learned that the original published amino-acid sequence (Ozols & Strittmatter, 1969) of bovine cytochrome was incorrect, and that the amidation states of three residues, 11, 13 and 57 had to be changed from Gln, Glu and Asp to Glu, Gln and Asn, respectively (Christiano & Steggle, 1989). Since these changes were essentially isostructural with respect to X-ray diffraction, they were incorporated into the model without perturbing the refinement.

The *X-PLOR* programs allowed refinement of alternate conformations for side chains where branching of density had been observed. After simulated annealing, model evaluation and some solvent modelling, alternate positions were included for two residues, Lys19 and Glu69. After refinement of the disordered side chains the maps showed negative density for the second site of Lys19; therefore, a series of SA omit maps was undertaken for regions where disorder was observed (Hodel *et al.*, 1992). The omit maps showed that there were two conformers for residues Glu44, Glu48, Glu69, Val61 and Ile75 but that Lys19, Lys28 and Glu56 had at least three conformers. Alternate conformations of surface side chains are frequently observed in high-resolution structures (Smith, Hendrickson, Honzatko & Sheriff, 1986) and discrete substates seem to be preferred over continuous perturbation. For cytochrome *b*₅ the electron density for residues with multiple conformers showed branching at *C*_β and *C*_γ. Since the positions for the remaining atoms of these side chains were ambiguous, only the major conformer for each was used and the occupancy was reduced. Alternative hydrogen-

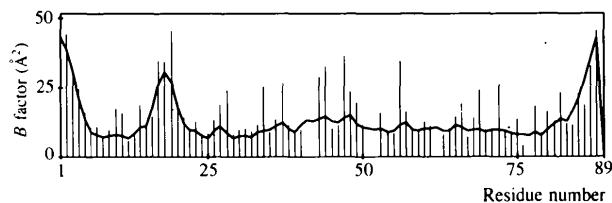


Fig. 4. Temperature factors of main- and side-chain atoms plotted as a function of the residue number. Average *B* values for the main-chain residues are represented by the continuous line while average *B* values for the side chains are shown as vertical lines. The average *B* value for main-chain atoms was 13 Å², for side-chain atoms 17 Å², the heme group 12 Å² and the solvent atoms 39 Å².

Table 4. β -Bends

Bend	Residues $n - n + 3$	Dihedral angles ($^{\circ}$)				Class*	Hydrogen-bond distances (\AA) $O_n \cdots N_{n+3}$
		$\varphi n + 1$	$\psi n + 1$	$\varphi n + 2$	$\psi n + 2$		
1	12-15	-103	-19	-82	-14	I	3.05
2	17-20	-62	-16	-78	-27	I	2.70
3	25-28	50	47	72	3	I'	2.89
4	39-42	-62	-26	-88	6	I	2.92
5	49-52	-61	140	85	9	II	3.21

* Classified according to Venkatachalam (1968).

bonding patterns could be invoked to explain the alternate positions of the polar side chains. However, there was no obvious explanation for the pairs of positions observed for Val61 and Ile75. Fig. 5 shows the electron density surrounding the side chain of Val61, in which a third node can be seen clearly. This type of density was observed for each of the residues which were modelled with disorder.

Many attempts were made to extend the model beyond residue 88. Unexplained density in the solvent regions of the crystal might be attributable to the remaining peptides. However, it did not prove possible to model Lys89 or Pro90 with confidence and connect them to the remaining peaks. Low-resolution data were included in attempts to refine models of this region.

When the final models, resulting from the *PROFFT* and *X-PLOR* refinements, are compared the $C\alpha$ atoms superimpose with a root mean square of 0.10 \AA . The greatest differences occur near the ends of the chain and in the β -bend region of residues 17-20. Of the 91 water molecules from the *PROFFT* refinement 84 persisted in the *X-PLOR* model, while the remaining seven sites now correspond to density for the extra three residues of the final model or alternate positions of side chains.

The Ramachandran plot (Fig. 3) of φ versus ψ angles for the final refined model shows that only two residues,

other than glycine, fall outside the energetically most favored region of the plot which corresponds to regular right-handed helices or β -sheet structure (Morris, MacArthur, Hutchinson & Thornton, 1992). The first of these, His26, lies at $\varphi = 47$ and $\psi = 49^{\circ}$, which is near the left-handed helical region. The second, Tyr27 has $\varphi = 71$ and $\psi = 0$. Both of these residues are part of the third β -bend (see Table 4), classified as type I' (Lewis, Momany & Scheraga, 1973). Sibanda, Blundell & Thornton (1989) further classified this bend as type I'2:2. Of 62 proteins surveyed, 16 exhibited this type of bend, 13 of which had Gly in position 2 and a residue tolerant of a left-handed helical conformation in position 1. The observed Ramachandran angles for both residues are similar to those found in the triple mutant of cytochrome *b*₅ (Funk *et al.*, 1990).

3.2. Structure of the molecule

The conformation of cytochrome *b*₅ at 2.0 \AA resolution has been described previously (Mathews *et al.*, 1971, 1979). Shown schematically in Fig. 6, the structure is approximately cylindrical with a length of about 37 \AA and a diameter of about 31 \AA . It contains six helices and five β -strands (Fig. 1). The heme group is held in a hydrophobic pocket at one end of the molecule and is coordinated to two histidine side chains. The heme-binding pocket is surrounded by four helices and is lined with hydrophobic side chains. The heme group extends about halfway into the molecule. A five-stranded β -sheet separates the heme-binding pocket from a second hydrophobic region at the other end of the molecule.

The detailed conformation of the six helices is presented in Table 5. Two different criteria were used to define the range of each helix. One, based on the $C\alpha$ backbone conformation (Levitt & Greer, 1977), is consistent with visual inspection of the molecule. The other is based on the hydrogen-bonding pattern.

Helix 4 is the most regular α -helix. The φ and ψ angles lie close to the expected values and there are no main-chain hydrogen-bonding interactions with solvent or side-chain atoms. The other helices are less regular and include hydrogen-bonding interactions with water molecules or side-chain atoms which disrupt the intra-

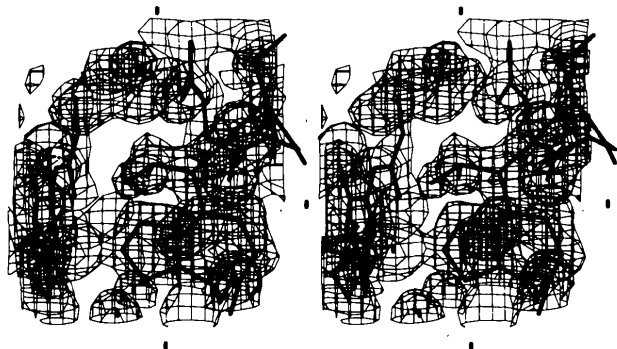


Fig. 5. Box of electron density surrounding Val61. The $2F_o - F_c$ map is contoured at a 1σ level and shows the four lobes of density around $C\beta$. The model is shown with only the principal conformer. (The unfilled density in the foreground results from a symmetry-related molecule.)

helical hydrogen-bonding pattern. Helix 2 is the most distorted, with four interactions to water or side-chain atoms. This helix is identified as a series of turns by the analysis program *DSSP* (Kabsch & Sander, 1983). Helix 6 is a 3_{10} helix, and is identified as such by *DSSP*. It also interacts with three water molecules and a side-chain atom. Helices 1, 3 and 5 begin as α -helices and convert to turns at the point where a central carbonyl O atom forms a hydrogen bond to a water or side-chain O atom, as indicated in Table 5. The occurrence of hydrated helices in proteins has often been observed (Sundaralingam & Sekharudu, 1989).

The five β -strands form a mixed β -sheet. The hydrogen-bonding pattern of this sheet is shown in Fig. 7. The central β -strand is antiparallel to each of the two adjacent outer pairs of parallel β -strands. The β -sheet, which contains two irregularities, is twisted to form part of a barrel-like structure. Strand $\beta 5$ exhibits a β -bulge (Richardson, Getzoff & Richardson, 1978). The peptide N atom of Gly77 in this strand is too far (3.55 Å) from the carbonyl of Val29 in strand $\beta 3$ to form a hydrogen bond; It is shielded from solvent and is not involved in any hydrogen bond. The other irregularity is in strand $\beta 4$ where the peptide N atom of Gly52 does not form a hydrogen bond to strand $\beta 2$ but is involved in a β -bend instead.

There are four β -bends in cytochrome b_5 . These are listed in Table 4 and classified according to Lewis *et al.*

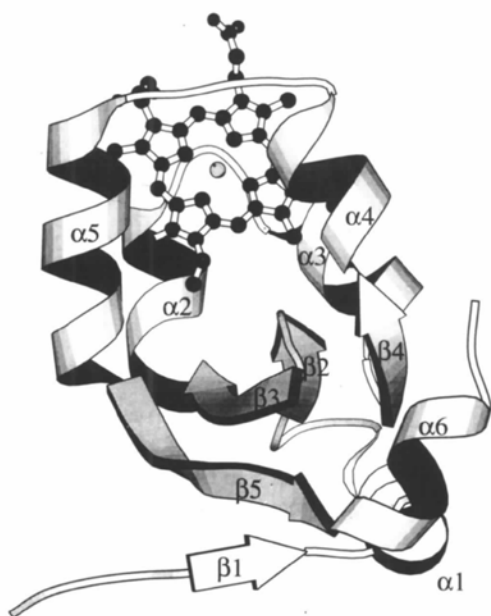


Fig. 6. *MOLSCRIPT* (Kraulis, 1991) diagram of cytochrome b_5 . The six helices are represented as coils, the five β -strands are represented as ribbons. Helix 2 (residues 33–38), helix 3 (residues 43–49), helix 4 (residues 55–60) and helix 5 (residues 65–74) are packed around the heme. The five β -strands, below the heme pocket, form a β -pleated-sheet structure in the center of the molecule.

(1973). The first bend occurs just before strand $\beta 2$ and the second between strands $\beta 2$ and $\beta 3$ (see Figs. 1 and 6). The third bend occurs between helices II and III while the fourth is located between helix III and strand $\beta 4$. Two other β -bends, identified previously (Mathews & Czerwinski, 1985), have been included as the beginnings of helices II and VI (Table 5). *DSSP* classified 71–74 as a fifth bend, but this has been included as part of helix 5.

There are 22 hydrogen bonds between side- and main-chain atoms listed in Table 6. There are an additional 15 side-chain to side-chain hydrogen bonds listed in Table 7. Seven of these are salt bridges between lysine or arginine and glutamate or aspartate residues. Three others are potential salt bridges involving histidine and glutamate residues depending on the protonation state of the former.

3.3. Heme group

In the 2.0 Å resolution MIR map a distinct non-planarity was observed in the electron density for the heme moiety (Mathews *et al.*, 1979). During the *PROFFT* refinement the heme group was not restrained to lie in a single plane: rather, each of the four pyrrole rings was restrained to a local plane. As a result of this refinement the heme group was distinctly non-planar. Pyrrole rings A and D had the greatest deviation from overall planarity and were twisted in opposite directions. There is very little change in the heme conformation between the model refined by *PROFFT* and that refined in *X-PLOR*. The heme group with its surrounding electron density is shown in Fig. 8 and a stereoview in Fig. 9 shows the twisting of the heme moiety.

The heme group is bound to cytochrome b_5 by coordination of the heme Fe atom to the N_{ϵ} atoms of two histidine side chains, His39 and His63. The surroundings of the heme group are presented in Table 8. Most of the heme group is buried in a hydrophobic pocket and forms

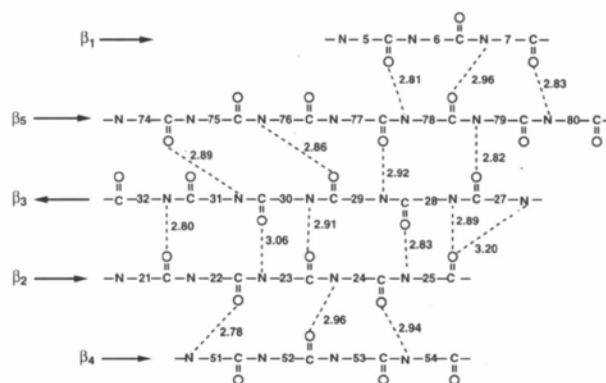


Fig. 7. Schematic diagram of the β -pleated-sheet bonding pattern. The arrows on the left show the direction of the strand. The hydrogen bonds are shown by dashed lines, the distances are given in Å.

Table 5. *Helices*

Helix	Backbone conformation	Hydrogen bonding	O	N	Distance (Å)	Comments
I	9–14	8–15	8	12	2.97	
			9	13	2.93	
			11	14	3.08	O10 interacts with water 502 at 2.85 Å, breaking the hydrogen-bond pattern
			12	15	3.05	
II	33–38	32–39	32	35	2.85	O32 forms a bifurcated hydrogen bond
			32	36	3.09	O33 interacts with two water molecules (517 at 2.97 and 589 at 3.00 Å)
			35	38	2.82	O34 interacts with water 521 at 2.87 Å and the symmetry related Asn13 at 3.04 Å
			35	39	3.02	O35 forms a bifurcated hydrogen bond
III	43–49	43–50	43	47	2.94	
			44	48	2.92	O45 interacts with water 524 at 2.86 Å breaking the hydrogen bond pattern
			46	49	3.01	O46 forms a bifurcated hydrogen bond
			46	50	3.25	
IV	55–60	54–60	54	58	2.93	
			55	59	2.98	
			56	60	2.78	
V	65–74	64–74	64	68	3.05	
			65	69	2.91	
			66	70	2.99	O66 interacts with water 520 at 2.87 Å but does not break hydrogen-bond pattern
			67	71	3.06	
			69	72	3.25	O68 to O71 hydrogen bond at 2.62 Å breaks the hydrogen-bond pattern
			70	73	3.09	
			71	74	2.97	
VI	81–86	80–87	80	83	2.87	This is a 3 ₁₀ helix
			81	84	3.21	O81 interacts with water 529 at 2.82 Å disrupting the hydrogen-bond pattern
			83	86	3.02	O82 interacts with waters 529 at 3.28 and 601 at 2.64 Å
			84	87	3.14	

Table 6. *Side-chain–main-chain hydrogen bonds*

Side-chain atom	Main-chain atom	Distance (Å)
Lys5 NZ	Ile76 O	2.71
Tyr7 OH	Ile76 O	3.46
Thr8 OG1	Glu11 N	3.13
Asn17 OD1	Lys19 N	3.25
Thr21 OG1	Asn17 O	2.78
Asp31OD1	Thr33 N	3.15
Thr33 OG1	Thr21 N	2.92
His39 ND1	Gly42 O	2.75
Arg47 NH2	Ser18 O	3.04
Asp53 OD1	Ile24 O	3.33
Asp53 OD1	Thr55 N	3.45
Thr55 OG1	His26 N	2.87
Asp60 OD1	Glu56 O	3.33
Asp60 OD2	Glu56 O	3.40
His63 ND1	Phe58 O	2.71
Ser64 OG	Asp66 N	3.21
	Ala67 N	3.07
Ser71 OG	Arg68 O	2.62
Thr73 OG1	Leu70 O	3.32
Asp83 OD2	Leu9 N	2.83
Arg84 NE	Leu79 O	2.93
Arg84 NH2	Leu79 O	2.81

Table 7. *Side-chain–side-chain hydrogen bonds*

Side-chain atom	Side-chain atom	Distance (Å)
Lys5 NZ	Tyr7 OH	2.67
Glu11 OE1	Lys14 NZ	3.40
Glu11 OE2	His15 NE2	2.89
His15 ND1	Ser20 OG	2.84
Trp22 NE1	Asp31 OD2	3.51
His26 NE2	Glu59 OE2	2.77
Asp31 OD1	Thr33 OG1	2.64
Flu43 OE2	Arg47 NH1	2.87
Glu49 OE1	Asn57 OD1	3.49
Asp53 OD1	Thr55 OG12	2.62
Glu59 OE1	Arg68 NH2	2.94
Glu59 OE2	Arg68 NH1	2.95
Glu78 OE1	Arg84 NH2	2.83
His80 NE2	Asp82 OD2	3.28
Asp83 OD1	Lys86 N2	2.79

van der Waals contacts with a number of non-polar side chains. One of the two propionic acid side chains of the heme extends into solution while the other is hydrogen bonded to the main- and side-chain atoms of Ser64.

Six atoms of the heme moiety have significant solvent accessibility, CAA, CGD, CMD, CBA, O1D and

O2D, (14, 21, 25, 25, 38 and 40 Å², respectively). These calculations were carried out according to Lee & Richards (1971) using half van der Waals radii (Brünger, 1990) and with solvent molecules omitted from the model. The heme propionate groups interact with seven solvent molecules (Table 8). Atoms O1A and O2A form hydrogen bonds to discrete solvent molecules, even though their accessibility to bulk solvent is calculated to be 5 and 0 Å², respectively. The propionate O atom O2A forms two hydrogen bonds to waters which are involved in a solvent network with each other and with another solvent molecule; the latter in

Table 8. Residues of the heme binding pocket and their distances of closest approach

Heme atom	Residue	Distance (Å)
C2B	Phe35 CE2	3.49
Fe	His39 NE2	2.07
C3D	Gly39 CA	3.46
CBC	Val45 O	3.22
CHC	Phe58 CD1	3.52
Fe	His63 NE2	2.00
O1A	Ser64 OG	2.71
O2A	Ser64 N	2.84
Water to heme distances (Å)		
O1A	H2O550 OH2	3.04
O2A	H2O598 OH2	2.79
O1D	H2O536 OH2	2.68
O2D	H2O588 OH2	3.14
O2A	H2O509 OH2	3.14
O1D	H2O545 OH2	3.19
O2D	H2O543 OH2	3.11

turn is hydrogen bonded to the heme propionate O1D. This network of waters, shown in Fig. 10, also forms hydrogen bonds to the protein backbone and to side-chain atoms of a symmetry-related molecule. One of the solvent molecules in this network, 509, is of considerable interest since it makes the closest solvent approach to the heme Fe atom (5.39 Å). The molecule forms four hydrogen bonds: to O2A (3.14 Å), to 61 O (2.79 Å), and to waters 598 at (2.70 Å) and 536 at (2.93 Å). The solvent accessibility of both the propionate O2A and water 509 remains zero, whether or not, waters are included in the calculations. All the solvent molecules which are associated with the heme group, except water 588, appear in identical positions in both the *PROFFT* and *X-PLOR* models.

In the original interpretation of the 2.8 Å resolution electron-density map (Mathews *et al.*, 1972) portions of the heme were poorly resolved leading to an incorrect choice for its orientation, with the positions of pyrrole

ring A and B interchanged with those of pyrrole rings D and C, respectively (Mathews, 1980). In solution, native cytochrome *b₅* has been found to exist in two distinct conformational states which differ in the way the heme group is oriented within the heme binding pocket (Walker, Emrick, Rivera, Hanquet & Buttlair, 1988; La Mar, Burns, Jackson, Smith & Strittmatter, 1981). In one conformation, which occurs about 90% of the time, the heme is oriented as shown in Fig. 6 while in the other, the heme group is rotated by 180° about a line connecting 1CH—3CH. In the crystal structure of the triple mutant of cytochrome *b₅* both heme conformations were observed with about equal occupancy (Funk *et al.*, 1990). In order to verify that the heme conformation found in the native structure is indeed correct, an omit map was calculated with half the heme group, corresponding to pyrrole rings A and B removed from the model. The resultant electron density clearly showed only one conformation for the heme vinyl groups indicating that the scattering from the minor component at the 10% level was insufficient to perturb the electron density. The heme orientation was further confirmed in a second map calculated with only the heme vinyl Cβ atoms removed. These results suggest that the heme binding disorder observed in the triple mutant arises from a subtle destabilization of the mutant protein structure with respect to the native protein.

3.4. Solvent structure

The final model of cytochrome *b₅* includes 117 solvent molecules (numbered from 501 to 617) with rankings which were inversely correlated to their temperature factors at the midpoint of the refinement. 11 of these water molecules have zero solvent accessibility with 17 more having minimal access to bulk solvent (< 5 Å²). These waters are located in grooves on the protein surface, or are themselves 'caged in' by other solvent molecules. Fig. 11 shows the distribution of solvent molecules around the protein.

A surface pocket is formed at the sheet end of the molecule. The backbone of Tyr30 is a central component of β₃; however the side chain points toward a pocket on the protein surface. The hydroxyl of this residue is bound tightly to two inaccessible waters, 516 and 534, which in turn bind to two other waters which are fully accessible to solvent. This rim of this pocket is rich in basic residues (His26, Lys28, Arg68 and Lys72) and hydrophobic groups (Leu25 and Ile75).

The solvent regions of the electron-density maps still show considerable unexplained density. The highest five peaks in the final $F_o - F_c$ map all lie close to O atoms and could not be modelled as simple solvent nor as phosphate anions. The strongest peak is 4.5σ and is situated just 1.2 Å from water 506; similarly the four remaining peaks lie less than 2.5 Å from waters 511, 512, 518, 522 and 528. The extra density near these

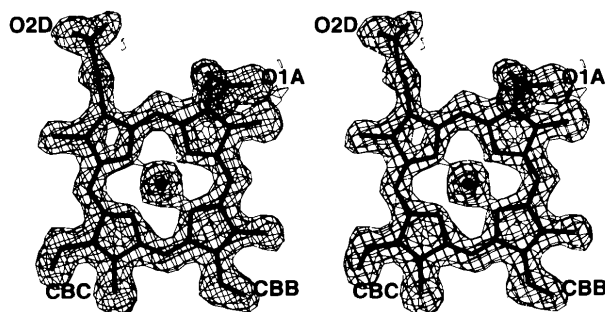


Fig. 8. Stereoview of the heme moiety showing the surrounding electron density. The $2F_o - F_c$ map was calculated using phases from the final *X-PLOR* refinement and was contoured at 1.5σ .

waters cannot be explained by large vibrational modes; in fact these waters have temperature-factor values which are below average. Attempts were made to model these strands of density as pairs of disordered water molecules; indeed a water network could be generated with 12 or more components. However, refinement collapsed these alternate waters to their original sites. The third peak (4σ) lies close to the protein, 1.8 Å from the hydroxyl O atom of Tyr27. The electron density surrounding this tyrosine is planar but extends beyond the hydroxyl group and downwards away from the plane. The Tyr27 OH forms a hydrogen bond to a symmetry-related molecule in the crystal and is in the proximity of solvent 522 mentioned above. Huntley & Strittmatter (1972) had shown that only three of the four tyrosine residues were chemically reactive and had identified Tyr27 as being the inactive residue. The peak in the difference map is at a distance which would be predicted for a P atom if the tyrosine had been phosphorylated. One water site could be part of this group, but there is insufficient room for two additional O atoms.

3.5. Crystal packing

The intermolecular contacts between protein molecules are tabulated in Table 9. Many of the highest peaks, first identified as solvents, were found bridging symmetry-related molecules. Each molecule of cytochrome *b*₅ interacts with three other symmetry-related molecules.

The strand β_1 , at the amino-terminal end of the protein (Fig. 6), packs against the rim of the heme cleft of an adjacent molecule related by translation along *z*. 16 bridging solvent molecules have been identified in this interface and these include 536, 543, 545, 575 and 598 which form bonds to propionate O atoms as described earlier. Three of the four bonds between the protein molecules at this interface involve main-chain atoms. This packing could best be described as head to tail. A second type of interaction, tail to tail, involves the β -sheet end of each molecule, related by a screw rotation parallel to *z*, and includes two salt bridges. This interface only contains three waters. The third interface contains one salt bridge, the strongest to occur as a result of crystal packing. This interface involves the surfaces of the helices which pack together in a side by side manner, related by screw rotation about the *y* axis. Three of the remaining five residues not involved in the salt bridge are each involved in two hydrogen bonds, all of which appear to be quite strong. There are eight waters in this region.

4. Concluding remarks

Investigations using a variety of techniques such as ¹H-NMR, laser flash-photolysis and infra-red spectroscopy, have shown that cytochrome *b*₅ forms

Table 9. Intermolecular contacts

Residue	Residue	Distance (Å)
Ser1 OG	Asp66 ⁱ OD1	3.27
Lys5 NZ	Gly62 ⁱ O	3.22
Tyr6 O	Glu59 ⁱ O	3.34
Tyr6 O	Gly62 ⁱ N	2.98
Thr8 N	Asp60 ⁱ O	3.12
Val4 O	Tyr27 ⁱⁱ OH	2.97
Tyr6 OH	His26 ⁱⁱ ND1	2.91
Lys28 NZ	Asp82 ⁱⁱ OD2	3.10
Glu59 OE1	Arg84 ⁱⁱ NH1	3.40
Gln13 O	Thr73 ⁱⁱⁱ OG1	2.54
Gln13 NE2	Lys34 ⁱⁱⁱ O	3.04
Asn16 OD1	Glu69 ⁱⁱⁱ O	2.86
Asn16 OD1	Thr73 ⁱⁱⁱ OG1	2.86
Glu38 OE2	Lys86 ⁱⁱⁱ NZ	2.68

Symmetry operators: (i) translation along *z* to (*x*, *y*, *z* - 1); (ii) Rotation by 2₁ parallel to *z* followed by translation along *x* to ($3/2 - x$, $1 - y$, $z - 1/2$); (iii) Rotation by 2₁ parallel to *y* followed by translation along *z* to ($1 - x$, $1/2 + y$, $3/2 - z$).

weak complexes with other electron-transfer proteins including cytochrome *c* (Stonehuerner, Williams & Millett, 1979; Hartshorn, Mauk, Mauk & Moore, 1987), cytochrome P₄₅₀ (Tamburini, White & Schenkman, 1985), myoglobin (Livingston, McLachlan, La Mar & Brown, 1985) and methemoglobin. These data suggest that electrostatic forces are involved in complex formation and that as solvent is excluded from the protein-protein interface hydration forces are replaced by salt linkages (Rogers, Pochapsky & Sliagar, 1988; Mauk, Barker & Mauk, 1991; Kornblatt, Kornblatt, Hoa & Mauk, 1993). Computer models of such complexes (Salemme, 1976; Poulos & Mauk, 1983; Wendoloski, Mathew, Weber & Salemme, 1987), together with mutagenic studies, have identified negatively charged groups on *b*₅ which link with positively charged residues surrounding the heme pocket of its partners. The solvent-exposed heme propionate and negatively charged residues on the cytochrome *b*₅ surface, specifically Glu43, Glu44, Glu48 and Asp60 were the first residues identified as forming linkages in these complexes. Both kinetic and NMR studies of the *b*₅-*c* complexes (Whitford, Concar, Veitch & Williams, 1990; Meyer *et al.*, 1993) confirmed that ionic strength modulates the formation and stability of the binary interactions and showed that there was considerable rotation of the partners in the complex.

The flexibility and variety of electron-transfer complexes involving cytochrome *b*₅ illustrate the difficulty in explaining electron transfer with a simple static model. The crystal structure of cytochrome *b*₅ shows that this protein provides a stable framework which permits considerable movement of the surface polar residues with little disruption of the polypeptide chain. This feature may render adaptability for cytochrome *b*₅ to form complexes with a variety of partners.

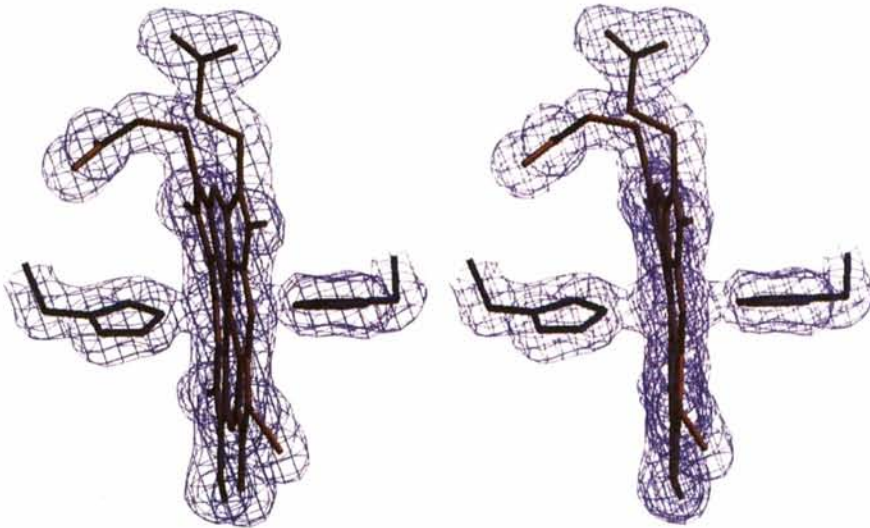


Fig. 9. Stereoview of the heme group, rotated from Fig. 8, illustrates the twisting of rings A and D out of the heme plane. The contour level of the $2F_o - F_c$ map is 1.0σ .

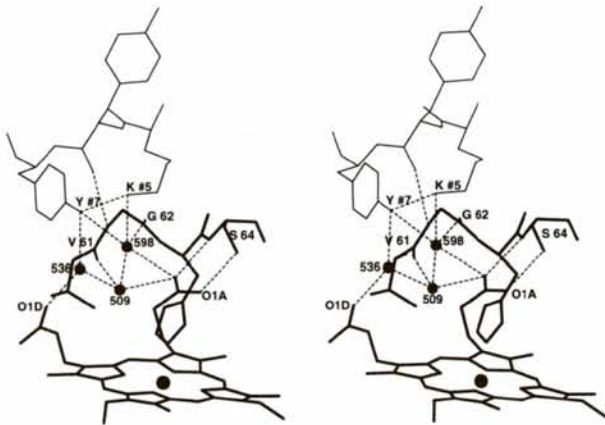


Fig. 10. Hydrogen-bonding network involving both heme propionates, 3 water molecules and the backbone atoms of residues 61–64. Residues #5–#7, shown in thin lines, are from a symmetry-related molecule and are involved in the network.

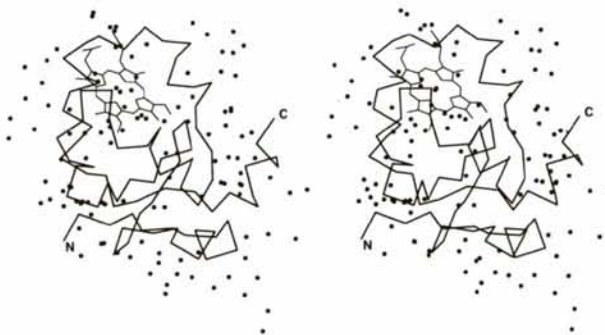


Fig. 11. Stereoview of the solvent distribution around the cytochrome molecule. The $C\alpha$ backbone is shown in the same orientation as Fig. 6.

This work has been funded by the National Institutes of Health, grant number GM20530.

References

- Beck von Bodman, S., Schuler, M. A., Jollie, D. R. & Sligar, S. G. (1986). *Proc. Natl. Acad. Sci. USA*, **83**, 9443–9447.
- Brünger, A. T. (1990). *X-PLOR Manual*, Version 2.1, Yale University, New Haven, Connecticut, USA.
- Christiano, R. J. & Stegles, A. W. (1989). *Nucleic Acids Res.* **17**, 799.
- Dailey, H. A. & Strittmatter, P. (1979). *J. Biol. Chem.* **254**, 5388–5396.
- Diamond, R. (1971). *Acta Cryst.* **A27**, 436–452.
- Enoch, H. G. & Strittmatter, P. (1979). *J. Biol. Chem.* **254**, 8976–8981.
- Estabrook, R. W., Hildebrandt, A. G., Baron, J., Netter, K. J. & Leibman, K. (1971). *Biochem. Biophys. Res. Commun.* **42**, 132–139.
- Finzel, B. C. (1987). *J. Appl. Cryst.* **20**, 53–55.
- Funk, W. D., Lo, T. P., Mauk, M. R., Brayer, G. D., MacGillivray, R. T. A. & Mauk, G. A. (1990). *Biochemistry*, **29**, 5500–5508.
- Guiard, B., Groudinsky, O. & Lederer, F. (1974). *Proc. Natl. Acad. Sci. USA*, **71**, 2539–2543.
- Guiard, B. & Lederer, F. (1979a). *Eur. J. Biochem.* **100**, 441–453.
- Guiard, B. & Lederer, F. (1979b). *J. Mol. Biol.* **135**, 639–650.
- Hartshorn, R. T., Mauk, A. G., Mauk, M. R. & Moore, G. R. (1987). *FEBS Lett.* **213**, 391–395.
- Hegesh, E., Hegesh, J. & Kaftory, A. (1986). *N. Engl. J. Med.* **314**, 757–761.
- Hendrickson, W. A. & Konert, J. (1980). *Biomolecular Structure, Function, Conformation and Evolution*, edited by R. Srinivasan, Vol. 1, pp. 43–57. Oxford: Pergamon Press.
- Hodel, A., Kim, S.-H. & Brünger, A. T. (1992). *Acta Cryst.* **A48**, 851–858.

- Holloway, P. W. & Katz, J. T. (1972). *Biochemistry*, **11**, 3689–3696.
- Hultquist, D. E. & Passon, P. G. (1971). *Nature (London)*, **229**, 252–254.
- Huntley, T. E. & Strittmatter, P. (1972). *J. Biol. Chem.* **247**, 4648.
- Jones, A. T. (1985). *Methods Enzymol.* **115**, 157–171.
- Kabsch, W. & Sander, C. (1983). *Biopolymers*, **22**, 2577–2637.
- Kornblatt, J. A., Kornblatt, M. J., Hoa, G. H. & Mauk, A. G. (1993). *Biophys. J.* **65**, 1059–1065.
- Kraulis, P. J. (1991). *J. Appl. Cryst.* **24**, 946–950.
- La Mar, G. N., Burns, P. D., Jackson, J. T., Smith, K. M. & Strittmatter, P. (1981). *J. Biol. Chem.* **256**, 6075–6079.
- Le, K. H. D. & Lederer, F. (1983). *EMBO J.* **2**, 1909–1914.
- Lederer, F., Shrir, R., Guiard, B., Cortial, S. & Ito, A. (1983). *Eur. J. Biochem.* **132**, 95–102.
- Lee, B. & Richards, F. M. (1971). *J. Mol. Biol.* **55**, 379–400.
- Levitt, M. & Greer, J. (1977). *J. Mol. Biol.* **114**, 181–239.
- Lewis, P. N., Momany, F. A. & Scheraga, H. A. (1973). *Biophys. Acta*, **303**, 211–229.
- Livingston, D. J., McLachlan, S. J., La Mar, G. N. & Brown, W. D. (1985). *J. Biol. Chem.* **260**, 15699–15707.
- Luzzati, P. V. (1952). *Acta Cryst.* **5**, 802–810.
- Mathews, F. S. (1980). *Biochim. Biophys. Acta*, **622**, 375–379.
- Mathews, F. S. (1985). *Prog. Biophys. Mol. Biol.* **45**, 1–56.
- Mathews, F. S., Argos, P. & Levine, M. (1971). *Cold Spring Harbor Quant. Biol.* **36**, 387–395.
- Mathews, F. S. & Czerwinski, E. W. (1985). *Cytochrome *b*₅ and Cytochrome *b*₅ Reductase from a Chemical and X-ray Diffraction Viewpoint*, in *The Enzymes of Biological Membranes*, edited by A. N. Martonosi, Vol. 4, pp. 235–300. New York: Plenum Press.
- Mathews, F. S., Czerwinski, E. W. & Argos, P. (1979). *The X-ray Crystallographic Structure of Calf Liver Cytochrome *b*₅*, in *The Porphyrins*, Vol. VII, edited by D. Dolphin, pp. 107–147. New York: Academic Press.
- Mathews, F. S., Levine, M. & Argos, P. (1972). *J. Mol. Biol.* **64**, 449–464.
- Mauk, M. R., Barker, P. D. & Mauk, A. G. (1991). *Biochemistry*, **30**, 9873–9881.
- Meyer, T. E., Rivera, M., Walker, F. A., Mauk, M. R., Mauk, A. G., Cusanovich, M. A. & Tollin, G. (1993). *Biochemistry*, **32**, 622–627.
- Miyata, M., Nagata, K., Yamazoe, Y. & Kato, R. (1989). *Pharmacol. Res.* **21**, 513–520.
- Morris, A. L., MacArthur, M. W., Hutchinson, E. G. & Thornton, J. M. (1992). *Proteins*, **12**, 345–364.
- Oshino, N., Imai, Y. & Sato, R. (1971). *J. Biochem. (Tokyo)*, **69**, 155–167.
- Ozols, J., Gerard, C. & Nobrega, F. G. (1976). *J. Biol. Chem.* **251**, 6767–6774.
- Ozols, J. & Strittmatter, P. (1969). *J. Biol. Chem.* **244**, 6617–6618.
- Poulos, T. L. & Mauk, A. G. (1983). *J. Biol. Chem.* **258**, 7369–7373.
- Ramakrishnan, C. & Ramachandran, G. N. (1965). *Biophys. J.* **5**, 909–933.
- Richards, F. M. (1968). *J. Mol. Biol.* **37**, 225–230.
- Richardson, J. S., Getzoff, E. D. & Richardson, D. C. (1978). *Proc. Natl Acad. Sci. USA*, **75**, 2574–2578.
- Rogers, K. K., Pochapsky, T. C. & Sligar, S. G. (1988). *Science*, **240**, 1657–1659.
- Rogers, M. J. & Strittmatter, P. (1975). *J. Biol. Chem.* **250**, 5713–5718.
- Roussel, A. & Cambillau, C. (1991). *TURBO-FRODO. Silicon Graphics Geometry Partners Directory*, p. 86. Mountain View, CA, USA: Silicon Graphics Inc.
- Salemme, F. R. (1976). *J. Mol. Biol.* **102**, 563–568.
- Sibanda, B. L., Blundell, T. L. & Thornton, J. M. (1989). *J. Mol. Biol.* **206**, 759–777.
- Slaughter, S. R., Williams, C. H. & Hultquist, D. E. (1982). *Biochim. Biophys. Acta*, **705**, 228–237.
- Smith, J. L., Hendrickson, W. A., Honzatko, R. B. & Sheriff, S. (1986). *Biochemistry*, **25**, 5018–5027.
- Spatz, L. & Strittmatter, P. (1971). *Proc. Natl Acad. Sci. USA*, **68**, 1042–1046.
- Stonehucmer, J., Williams, J. B. & Millett, F. (1979). *Biochemistry*, **18**, 5422–5427.
- Strittmatter, P. & Ozols, J. (1966). *J. Biol. Chem.* **241**, 4787–4792.
- Strittmatter, P. & Velick, S. F. (1956). *J. Biol. Chem.* **221**, 253–264.
- Sundaralingam, M. & Sekharudu, Y. C. (1989). *Science*, **244**, 1333–1337.
- Tamburini, P. P., White, R. E. & Schenkman, J. B. (1985). *J. Biol. Chem.* **260**, 4007–4015.
- Utecht, R. E. & Kurtz, D. M. Jr (1988). *Biochim. Biophys. Acta*, **953**, 164–178.
- Venkatachalam, C. M. (1968). *Biopolymers*, **6**, 1425–1436.
- Walker, F. A., Emrick, D., Rivera, J. E., Hanquet, B. J. & Buttlaire, D. H. (1988). *J. Am. Chem. Soc.* **110**, 6234–6240.
- Wendoloski, J. J., Mathew, J. B., Weber, P. C. & Salemme, F. R. (1987). *Science*, **238**, 794–797.
- Whitford, D., Concar, D. W., Veitch, N. C. & Williams, R. J. (1990). *Eur. J. Biochem.* **192**, 715–721.
- Yoo, M. & Steggles, A. W. (1988). *Biochem. Biophys. Res. Commun.* **156**, 576–580.